EAI Endorsed Transactions
on Energy Web
Research Article EAI.EU

Enhanced Thrust Ripple Suppression Method in PMLM Using Indirect Adaptive Robust Control

Yuanfeng He[1], Weizhen Wang[2], Rong Li[2], Wenyuan Yan[2], Jiutong Yang[3], and Chi Zhang[2*]

[1]School of Electromechanical and Rail Transit, Zhejiang Fashion Institute of Technology, Ningbo, Zhejiang 315211, China
[2]Zhejiang Key Laboratory of Robotics and Intelligent Manufacturing Equipment Technology, Ningbo Institute of Materials Technology and Engineering, Chinese Academy of Sciences, Ningbo, Zhejiang 315201, China
[3]Suzhou Inovance Technology Co., Ltd., Suzhou, Jiangsu 215100, China

Abstract

INTRODUCTION: The indirect adaptive robust control (IARC) can effectively improve servo performance under external disturbances, including thrust ripple. In the conventional IARC method, the recursive least squares (RLS) treats the low-pass-filtered total control signal as the measured output. Such filtering introduces parameter estimation errors caused by phase lag in the measured signal, whereas direct filter removal results in algebraic loop issues.
OBJECTIVES: To address these limitations, a novel method using the indirect adaptive robust control with a measured-output-reconfigured RLS (IARC-MORRLS) is proposed in this paper.
METHODS: Firstly, the proposed method utilizes the feedback control signal directly as the measured output of RLS, thereby improving the accuracy of parameter estimation by mitigating phase-lag-induced errors. Then, a variable-gain mechanism is developed to guarantee the complete convergence of parameter estimates. Finally, a slope-judgment mechanism is incorporated into projection mapping to suppress oscillations in initial parameter estimation.
RESULTS: Simulations and experimental validations were used on a permanent magnet linear motor (PMLM) driven motion system. The validation experiment proves that IARC-MORRLS method proposed in this paper exhibits better performance in thrust ripple suppression over the conventional IARC method.
CONCLUSION: It will help PMLM system reach better performance under external disturbances.

Keywords: permanent magnet linear motor (PMLM); indirect adaptive robust control (IARC); recursive least squares (RLS); thrust ripple suppression; motion control

Received on 08 May 2026, accepted on 09 June 2026, published on 22 June 2026

doi: 10.4108/ew.12952

*Corresponding author. Email: zhangchi_paper@163.com

1. Introduction

1.1 Background of Research

The permanent magnet linear motors (PMLMs), notable for their rapid response capability and high-precision positioning, are essential components in modern industrial applications[1]. The direct-drive mechanism effectively reduces mechanical friction found in conventional ball screw feed system[2]. The PMLMs are primarily applied in high-speed magnetic levitation transportation[3], intelligent manufacturing systems[4] and logistics automation systems[5], driving advancements in efficiency and intelligent automation across industries. However, the permanent magnets and armature windings in PMLMs generate periodic thrust ripple because of the end effect and slot effect[6, 7]. Especially in the aspect of low-speed precision positioning applications, thrust ripple severely

compromises motion smoothness and control accuracy, impeding wider adoption of PMLMs. Therefore, effective thrust ripple suppression method is required. Current methods are categorized into two domains: motor-structure design optimization and control-strategy optimization. Motor-structure design optimization plays an important role in minimizing thrust ripple [8, 9] but cannot eliminate thrust ripple[10].

Recent studies have developed a variety of control strategy optimization methods. Zhu et al. utilized the field-oriented control (FOC) method by injecting predictive currents to permanent magnet linear synchronous motor (PMLSM) to compensate thrust ripples[11]. Zuo et al. discussed a direct thrust control method for multi-module PMLSM in automated warehousing application. The method employs a composite thrust reference with online optimization to suppress thrust ripple under dynamic conditions[12]. Yuan et al.[13] developed an enhanced PMLSM thrust differential model. This method implements an internal model controller with direct current compensation for ripple suppression. Fu et al.[14] researched inverse model iterative learning control (IMILC) and robust disturbance observer (RDOB). They combined IMILC's high tracking accuracy with RDOB's robustness and rapid convergence, effectively reduced inherent thrust ripple and enhanced system performance. Zhang et al.[15] proposed a novel method utilizing a combined model reference adaptive control and periodic adaptive learning control (MRAC-PALC) algorithm. The MRAC handles initial parameter acquisition, and the PALC updates parameters online in subsequent iterations, which estimates and compensates thrust ripple for repetitive motion tasks. Furthermore, recent advancements have continuously pushed the boundaries of disturbance suppression. Lee et al. [16] proposed a novel control method that adjusts D-axis and Q-axis currents to simultaneously reduce tangential and normal force ripples during dynamic acceleration. Specifically, their approach establishes a comprehensive force model incorporating cross-coupling effects and reluctance forces, enabling the analytical derivation of compensating currents through indirect experimental identification procedures without requiring dedicated force sensors. From an observer-based control perspective, Zhang et al. [17] developed a proportional resonant internal model extended state observer combined with iterative learning control to systematically eliminate both periodic detent forces and aperiodic residual disturbances. In this architecture, an iterative learning controller with a forgetting factor initially suppresses the dominant periodic ripples, while the internal model extended state observer augmented with a resonant term accurately estimates and compensates for complex unmodeled residual fluctuations in real time. Alongside these developments, Lu et al. [18] proposed a model that not only captures periodic characteristics of cogging force but also non-periodic characteristics. This model utilizes B-spline functions to enable online adaptive compensation, while also integrating an adaptive robust control (ARC) method. The ARC method combines the advantages of adaptive control (AC) and deterministic robust control (DRC) while avoiding their individual limitations[19]. This method is applicable to dynamic systems involving parameter uncertainties and uncertain nonlinearities. To overcome the limited estimation performance of the direct adaptive robust control (DARC) method, researchers developed the indirect adaptive robust control (IARC) method under an independent adaptation law[20].

The recursive least squares (RLS) adaptation law employed in conventional IARC defines the low-pass-filtered total control signal as the measured output[21, 22]. However, introducing such a filter introduces unexpected phase delay, which compromises both parameter estimation accuracy and controller performance. To resolve this issue, an IARC method with a measured-output-reconfigured RLS (IARC-MORRLS) is proposed. The proposed method redefines the feedback control signal as the measured output of RLS, thereby eliminating the need for a low-pass filter and preventing algebraic loop. This modification, however, introduces premature convergence in parameter estimation. Therefore, an analytical relationship between the feedback control signal and disturbance compensation signal is established. Based on this analysis, a variable-gain mechanism is formulated and integrated into the adaptation law. This method enhances disturbance estimation accuracy, and improves thrust ripple suppression. Then, similar to [21], a slope-judgment mechanism is added to the parameter projection, constraining parameter estimates within prior-knowledge-based bounds and imposing predefined limits on their update rates. Finally, the proposed method is thoroughly validated through simulations and experiments carried out on the same PMLM [23]. Comparative analysis confirms its efficacy.

The rest content of this paper is as follows: Section 2 introduces the controlled precision motion stage, establishes its nominal dynamic model, and analyzes thrust ripple characteristics. Section 3 details the proposed IARC-MORRLS method. Section 4 provides simulation validation. Section 5 describes the PMLM based servo experiment information and results. Section 6 makes the conclusion of the study.

1.2 Contributions

The contributions of this paper are listed below:

1) The IARC-MORRLS method enhances adaptive thrust ripple compensation by shifting measured output of RLS from total control signal to feedback control signal and eliminating low-pass filtering, thereby mitigating parameter estimation errors induced by phase lag in the measured signal.

2) The parameter adaptation law both incorporates a variable-gain mechanism to ensure better convergence of parameter estimates and integrates a slope-judgment mechanism into the projection mapping to attenuate initial-stage oscillations.

3) The proposed method combines an H_∞ robust feedback controller with a parameterized third-order feedforward compensation to achieve rapid trajectory tracking and improve control system robustness.

2. System Description And Dynamic Model

2.1 The Precision Motion Stage Structure

The controlled linear motor is referred to as a 12P12S PMLM, where xPyS means the number of poles is x and the number of slots is y. The 12P12S PMLM incorporates a novel topology characterized by the same number of poles and slots. Throughout the optimization design process, the application of Taguchi's method and Genetic Algorithm (GA) achieves the suppression of detent force while preserving high thrust density, consequently attenuating thrust ripple in the PMLM[23]. Fig. 1 illustrates the precision motion stage based on the 12P12S PMLM.

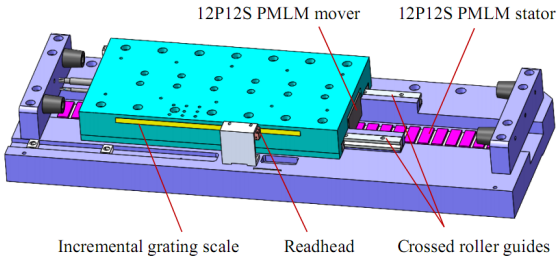

Figure 1. Structure of 12P12S PMLM based precision motion stage

The stage comprises crossed roller guides, an incremental grating scale with a readhead, and the 12P12S PMLM. The PMLM drives the integrated stage over a stroke of approximately 170 mm for trajectory tracking, while the grating scale provides position feedback with a resolution of 50 nm, thereby satisfying the stage's precision requirements.

2.2 Dynamic Modeling of the Stage

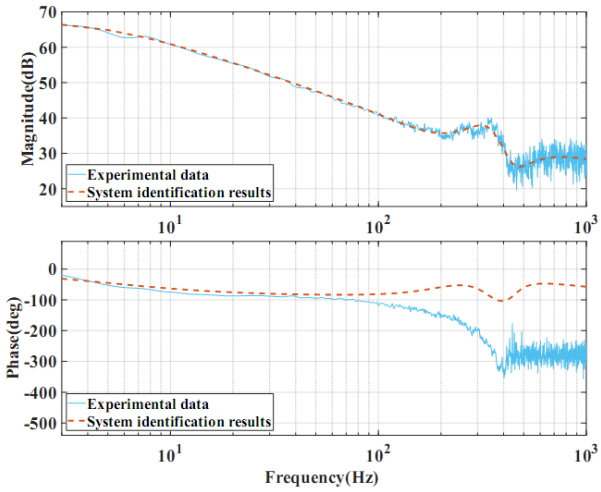

Figure 2. System identification of the controlled plant

The 12P12S PMLM is driven by a Coley driver which is configured in the current mode, forming the servo system controlled plant. After tuning, the current loop achieved a bandwidth of 1500 Hz. Fig. 2 are the System identification results.

In the amplitude-frequency characteristic of system identification results, the low-frequency rigid mode is modeled with a real pole, while high-frequency resonance/anti-resonance modes are represented by two complex-conjugate pole-zero pairs. This analysis yields the nominal controlled plant's transfer function:

$$G_n(s)=\frac{2.1054\times10^5 s^4+4.5536\times10^8 s^3+2.2800\times10^{12} s^2+2.5194\times10^{15} s+2.9073\times10^{18}}{s^5+5.9854\times10^3 s^4+1.7226\times10^7 s^3+3.1094\times10^{10} s^2+3.8142\times10^{13} s+1.1681\times10^{15}} \quad (1)$$

Eq. (1) accurately characterizes the controlled plant's amplitude-frequency response. While the phase response exhibits distinct high-frequency lag, this lag is compensable through time-delay compensation to enhance dynamic modeling precision[24]. This paper specifically focuses on low-speed operational conditions, under which the phase-frequency response requires sufficient matching exclusively in the low-frequency domain.

2.3 Thrust Ripple Analysis and Modeling

Experimental results confirm significant residual detent force in the 12P12S PMLM, with a theoretical period of 15 mm[23]. Analyzing the position-loop proportional-integral-derivative (PID) control output signal during constant low speed operation allows for indirect thrust ripple inference[25]. Thus, the Copley driver was configured in position control mode, and the linear motor operated at a constant low speed of 15 mm/s over a 160 mm stroke, with the corresponding PID control output presented in Fig. 3. A significant thrust ripple with a spatial period of approximately 15 mm is observed during controlled operation of the 12P12S PMLM. The associated amplitude-

phase nonlinearities are potentially attributed to assembly misalignment and the modular stator design inherent to this

specific 12P12S topology.

The thrust ripple model[26] is structured as follows:

$$F_r(x)=A^T S_r(x) \quad (2)$$

where x denotes the linear motor mover position, and

$$S_r(x)=\left[\sin\left(\frac{2\pi}{P}x\right),\cos\left(\frac{2\pi}{P}x\right),...,\sin\left(\frac{2\pi q}{P}x\right),\cos\left(\frac{2\pi q}{P}x\right)\right]^T \quad (3)$$

$$A_r=\left[A_{r1s},A_{r1c},...,A_{rqs},A_{rqc}\right]^T\in R^{2q} \quad (4)$$

Eq. (3) characterizes the harmonic spectrum of the thrust ripple model, with q indicating harmonic order and P designating pole pitch of motor. The corresponding weighting coefficients are specified in Eq. (4).

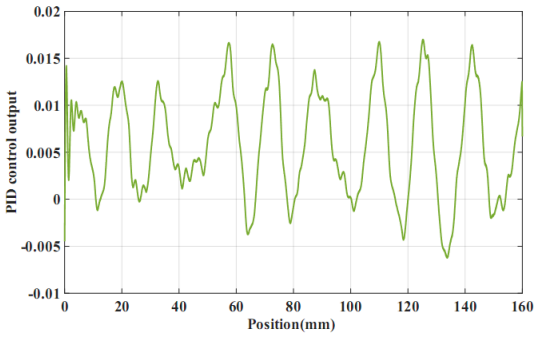

Figure 3. Experimental analysis of the thrust ripple

Such thrust ripple compromise motion control accuracy in 12P12S PMLM based motion stage. Consequently, this study develops a compensation method for active suppression of thrust ripple during motion tracking.

3. Iarc-Morrls Control Schemes

Fig. 4 is the schematic of the IARC-MORRLS method, where r_p , r_v , r_a and r_j denote the reference position trajectory, reference velocity trajectory, reference acceleration trajectory, and reference jerk trajectory, respectively; u_{fb} means the feedback signal, u_{atrc} is the adaptive thrust ripple compensation, u denotes the total control signal, and s denotes the differentiation of the signal.

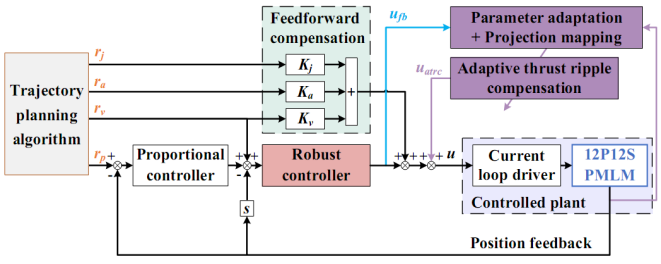

Figure. 4 Schematic of the proposed IARC-MORRLS method

S-curve trajectory planning is employed for point-to-point (PTP) motion, adopting the method described in [27]. The dual-loop feedback controller incorporates a position-loop proportional (P) controller and a velocity-loop robust controller, which makes the servo control system has enhanced stability and robustness. Notably, the proposed method structurally decouples reference trajectory components from the adaptive model compensation of conventional IARC methods [22]. Simultaneously, the adaptive thrust ripple compensation is retained. By reconfiguring the decoupled reference trajectory components into parameterized feedforward compensation, the proposed method simultaneously improves dynamic performance and enables focused estimation of disturbance-related parameters, achieving targeted thrust ripple suppression. Additionally, projection mapping is employed to prevent performance degradation caused by parameter oscillations during the adaptation process.

3.1 Robust Feedback Control and Parametrized Feedforward Compensation

The velocity-loop feedback controller employs a weighted hybrid sensitivity H_∞ robust control strategy to effectively attenuate disturbances within the proposed control scheme, as illustrated in Fig. 5, where $G_{vc}(s)$ denotes the robust controller, w denotes the input signal of reference velocity, e denotes the tracking error of velocity, u is the control signal, v is the measured output signal, $W_e(s)$, $W_u(s)$, and $W_v(s)$ are the weighting functions of e , u , v , respectively, and $z=\left[z_e,z_u,z_v\right]'$ is the corresponding weighted signal.

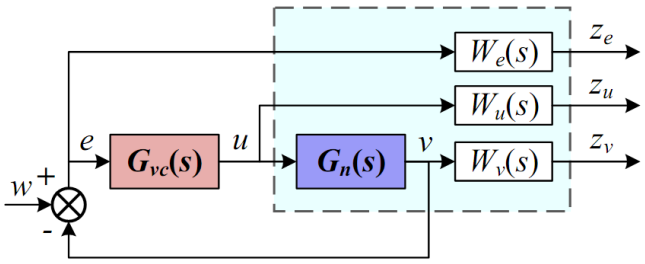

Figure 5. Schematic diagram of velocity-loop feedback control

The sensitivity functions are defined as follows:

$$S(s)=\left(I+G_{vc}(s)G_n(s)\right)^{-1} \quad (5)$$

$$R(s)=G_{vc}(s)\left(I+G_{vc}(s)G_n(s)\right)^{-1} \quad (6)$$

$$T(s)=I-S(s)=G_{vc}(s)G_n(s)\left(I+G_{vc}(s)G_n(s)\right)^{-1} \quad (7)$$

The closed-loop transfer function from w to z is given by:

$$T_{zw}(s)=\begin{bmatrix}W_e(s)S(s)\\W_u(s)R(s)\\W_v(s)T(s)\end{bmatrix} \quad (8)$$

Then, the stability controller is designed to satisfy the following conditions:

$$\left\| T_{zw}(s) \right\|_{\infty} < 1 \tag{9}$$

Weighting functions satisfying Eq. (9) are selected according to actual engineering experience, and the nominal plant model is designated as $G_n(s)$, for developing the weighted hybrid sensitivity H_{∞} robust controller. Eq. 10 is the transfer function of the obtained velocity-loop robust feedback controller:

$$G_{vc}(s) = \frac{3.8857\times10^{-2}s^5 + 2.3276\times10^{2}s^4 + 6.6991\times10^{5}s^3 + 1.2092\times10^{9}s^2 + 1.4840\times10^{12}s + 4.5448\times10^{13}}{s^5 + 2.1628\times10^{3}s^4 + 1.0829\times10^{7}s^3 + 1.1966\times10^{10}s^2 + 1.3809\times10^{13}s + 1.2270\times10^{11}} \tag{10}$$

To achieve fast trajectory tracking, a parameterized third-order feedforward compensation $F(s)$ is introduced:

$$F(s) = K_v + K_a s + K_j s^2 \tag{11}$$

where K_v, K_a, and K_j are the feedforward parameters for velocity, acceleration, and jerk, respectively.

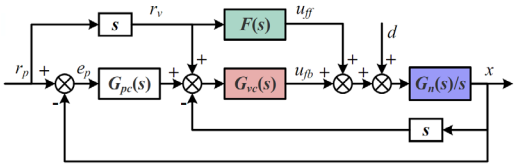

Figure 6. Schematic of the composite control method

Fig. 6 shows the composite control method that combines a dual-loop feedback controller and feedforward compensation, where $G_{pc}(s)$ denotes the position-loop feedback controller, d denotes the lumped external disturbance, x is the position output, e_p is the position tracking error, and u_{ff} is the feedforward signal of compensation. Without the feedforward compensation and disturbance d, the transfer function from r_p to x is defined below:

$$T_{xr}(s) = \frac{G_{pc}(s)G_{vc}(s)G_n(s)s^{-1} + G_{vc}(s)G_n(s)}{1 + G_{pc}(s)G_{vc}(s)G_n(s)s^{-1} + G_{vc}(s)G_n(s)} \tag{12}$$

Assuming nominal model invertibility, it can be inferred from Fig. 6 that:

$$e = \frac{G_n(s)s^{-1}}{1 + G_{cp}(s)G_{cv}(s)G_n(s)s^{-1} + G_{cv}(s)G_n(s)} \cdot \left((G_n(s))^{-1} - F(s) \right) r_v \tag{13}$$

Subsequently, the lumped disturbance d is incorporated. Through analyzing the dual-loop feedback controller, the transfer function from r_v to u_{fb} can be gained:

$$u_{fb} = -T_{xr}(s)d + T_{xr}(s) \cdot \left((G_n(s))^{-1} - F(s) \right) r_v \tag{14}$$

With the properly designed feedback controller, $T_{pr}(s)$ serves as a low-pass filter and can be approximated by unity gain within its bandwidth. As Eq. (13) shows, precise reference tracking is achieved when the parameterized feedforward compensation is tuned to approximate the nominal plant's inverse model[28], and the second term in Eq. (14) converges to 0. Thus, within the closed-loop bandwidth, the residual u_{fb} approximates the external disturbance compensation value.

3.2 Projection Mapping with Slope-Judgment Mechanism

Uncertain nonlinear disturbances in the servo system can induce unstable dynamics in parameter adaptation. This parametric instability severely degrades control precision with potential risk of closed-loop destabilization. Therefore, a coordination mechanism governing robust control and parameter adaptation needs to be synthesized. A widely adopted coordination mechanism employs projection mapping $\mathrm{Proj}_{\hat{\Theta}}(\bullet)$ to strengthen the adaptation law against uncertain nonlinearities[29]. Critical to the projection is the assumption of bounded disturbances and uncertain parameters:

$$\Theta \in \Omega_{\Theta} \triangleq \left\{ \Theta : \Theta_{\min} \le \Theta \le \Theta_{\max} \right\} \tag{15}$$

where $\Theta_{\max}$ and $\Theta_{\min}$ represent the theoretical upper and lower limits of the uncertain parameters, respectively. A definition of the projective mapping is given as follows:

$$\mathrm{Proj}(\hat{\bullet}_i) = \begin{cases} 0, & if\ \hat{\bullet}_i > \Theta_{i\max}\ and\ \dot{\hat{\bullet}}_i > 0 \\ 0, & if\ \hat{\bullet}_i < \Theta_{i\min}\ and\ \dot{\hat{\bullet}}_i < 0 \\ \dot{\hat{\bullet}}_i, & \text{otherwise} \end{cases} \tag{16}$$

where $\hat{\bullet}$ is the estimate of $\bullet$, and $\dot{\hat{\bullet}}$ is the estimated update rate of parameter. Projection mapping indicates that when the estimated value of an unknown parameter hits its predefined upper or lower bound while still maintaining an increasing or decreasing trend, the estimate is reset to 0; otherwise, the estimated value is retained. Theoretically, this mechanism prevents instability in the control system caused by excessively large or small parameter estimates. However, the estimated parameter may still oscillate within preset

bounds, compromising convergence rate and control performance. Therefore, under the conditions of Eq. (16), we define the constraint function as:

$$con_{\dot{\Theta}_m}(\hat{\bullet}) = c_0 \hat{\bullet}, \qquad c_0 = \begin{cases} 1, & \left|\dot{\hat{\bullet}}\right| \le \dot{\Theta}_m \\ 0, & \left|\dot{\hat{\bullet}}\right| > \dot{\Theta}_m \end{cases} \tag{17}$$

where $\dot{\Theta}_m$ denotes the predefined parameter update rate limit. Eq. (17) implements real-time slope judgment on the curves of estimated parameters to constrain excessive update rates, thereby mitigating parameter oscillations.

3.3 Measured-Output-Reconfigured RLS Adaptation Law with Variable-gain Mechanism

The nominal dynamic model described by Eq. (1) can be simplified to a rigid-body mode with only a first-order real pole, yielding the following reduced first-order model:

$$G_{n2}(s) = \frac{A_f}{Ms + B} \tag{18}$$

Accounting for external disturbances, specifically thrust ripple F_r, the frequency-domain model in Eq. (18) transforms into the following time-domain representation:

$$(M / A_f)\ddot{x} + (B / A_f)\dot{x} = u - F_r \tag{19}$$

where M denotes the inertia, B denotes the damping coefficient, and A_f represents the linear motor's driving force with A_f as the thrust constant and u as the total control signal. Subsequently, Eq. (19) can be expressed by the following linear regression form:

$$u = -\varphi^T \Theta \tag{20}$$

Where $\Theta = [\Theta_1, \Theta_2, \Theta_3]^T = [M / A_f, B / A_f, A_r^T]^T$ means the parameter set which is unknown and needs to be estimated, and $\varphi^T = [-\ddot{x}, -\dot{x}, -S_r(x)]$ is the measured input. The adaptive model compensation of the conventional IARC method[16] can then be designed as:

$$u_{amc} = -\varphi^T \hat{\Theta} \tag{21}$$

When utilizing the reference input trajectory as the measured signal, the term $-\hat{\Theta}_1\ddot{x} - \hat{\Theta}_2\dot{x}$ in Eq. (21) can be interpreted as acceleration and velocity feedforward compensation components.

This term is replaced by higher-order parameterized feedforward compensation as depicted in Fig. 4. Let $\phi_r = S_r(x)$, then the adaptive thrust ripple compensation is defined as follows:

$$u_{atrc} = -\varphi_r^T \hat{A}_r \tag{22}$$

Then, under the assumption stated in Eq. (15), the RLS adaptation law is employed to obtain accurate online parameter estimates for thrust ripple coefficient A_r. Following the principles of RLS, unknown parameters can be estimated given the measured input and output. However, estimating A_r would treat the unknown thrust ripple as the measured output, which directly violates causality.

In conventional IARC implementations, the measured output is set to the filtered total control signal [21, 22, 29]. Although omitting the low-pass filter avoids phase lag in the measured signal, it creates an algebraic loop. Conversely, introducing this filter inevitably degrades signal observation quality, which compromises thrust ripple compensation performance. Based on the analysis of Eq. (14) in Section 3.1, this paper proposes changing the measured output from the total control signal to the feedback signal u_{fb}, and removing the low-pass filter.

However, inducing such reconfiguration leads to premature convergence of the estimated parameters. Assuming no additional disturbances and properly tuned feedforward compensation, the feedback control signal $u_{fb}(t)$ in the time domain inherently contains implicit information regarding the external thrust ripple disturbance $d(t)$ prior to the implementation of compensation, as given by:

$$u_{fb}(0) \approx -d(0) \tag{23}$$

The thrust ripple compensation signal $\hat{d}(t)$ is then obtained by fitting u_{fb} as follows:

$$\hat{d}(t) \approx -u_{fb}(t) \tag{24}$$

During the parameter estimation process, as $\hat{d}(t)$ gradually approaches the actual thrust ripple, the disturbance components in u_{fb} will decrease:

$$u_{fb}(t) \approx u_{fb}(0) + \hat{d}(t) \tag{25}$$

Eq. (25) demonstrates that the residual component in $u_{fb}(t)$ plus $d(t)$ theoretically equals the uncompensated thrust ripple $u_{fb}(0)$. Since RLS serves as an online parameter estimation algorithm, the synthesis of Eq. (24) and Eq. (25) demonstrates that the thrust ripple compensation converges to equilibrium as follows:

$$u_{fb}(0) \approx 2u_{fb}(t) \approx -2\hat{d}(t) \tag{26}$$

In the equilibrium state, the amplitude of u_{fb} is approximately half the amplitude of the thrust ripple:

$$u_{fb}(t) \approx \frac{1}{2}u_{fb}(0) \approx -\frac{1}{2}d(0) \tag{27}$$

Thus, the parameter estimation for thrust ripple compensation achieves preliminary convergence, leaving approximately 50% of the thrust ripple uncompensated. Nevertheless, Eq. (27) indicates that doubling the parameters after preliminary convergence enhances estimation accuracy beyond conventional IARC method, owing to the elimination of the low-pass filter.

To guarantee the complete convergence of parameter estimates, a time threshold T_{th} is set. When T_{th} is exceeded, parameter estimation terminates and all estimated parameters are doubled. Since directly doubling these parameters introduces step-like disturbances, we develop the following variable-gain function:

$$\text{varg}_{T_{th}}(\hat{\bullet}) = c_1(t)\hat{\bullet}, \qquad c_1(t) = \begin{cases} 1, & 0 \le t \le T_{th} \\ 2 - R^{t-T_{th}}, & t > T_{th} \end{cases} \tag{28}$$

where $0 < R < 1$ determines the convergence rate of c_1. Eq. (28) implements a variable-gain mechanism that drives parameter estimates from preliminary convergence toward actual values beyond T_{th}, guaranteeing steady-state convergence. The update of the parameter estimate is carried out as the following measured-output-reconfigured RLS adaptation law:

$$L(k) = P(k-1)\varphi_r(k)\left[1 + \varphi_r^T(k)P(k-1)\varphi_r(k)\right]^{-1} \tag{29}$$

$$\hat{A}_r(k) = \hat{A}_r(k-1) + L(k)\left[-u_{fb}(k) - \varphi_r^T(k)\hat{A}_r(k-1)\right] \tag{30}$$

$$P(k) = \left[I - L(k)\varphi_r^T(k)\right]P(k-1), \qquad P(0) = p_0 I \tag{31}$$

Where $k \in Z^+$, L denotes the gain vector, P denotes the covariance matrix. Then, by applying the variable-gain mechanism, the slope-judgment mechanism, and projection mapping, the final estimate of A_r is obtained:

$$\hat{A}_r = \text{varg}_{T_{th}}\left(\text{con}_{\Theta_m}(\text{Proj}(\hat{A}_r))\right), \qquad \hat{A}_r(0) \in \Omega_\Theta \tag{32}$$

Consequently, the estimated parameters achieve reduced deviation from actual values compared to conventional IARC method, thereby enhancing thrust ripple compensation performance.

4. Simulation Verification

To validate the proposed IARC-MORRLS method, this section presents simulation results demonstrating the third-order S-curve trajectory tracking performance of the 12P12S PMLM under simulated thrust ripple conditions. The reference trajectory is shown in Fig. 7, where Dis denotes displacement, with its first to third derivatives labeled Vel (velocity), Acc (acceleration), and Jerk (jerk), respectively. The trajectory bounds adopted in the simulations are set to 0.5 m/s, 50 m/s^2, and 5100 m/s^3, respectively. Given the theoretical thrust ripple period of 15 mm, the stage is programmed to track trajectory within a 50 mm stroke, with real-time displacement monitored.

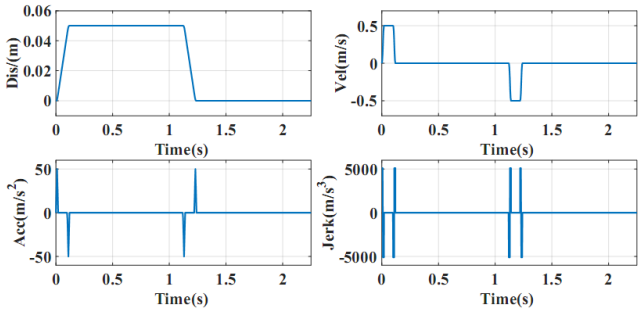

Figure 7. Reference trajectory used in simulation

The nominal model used in simulation is defined by Eq. (1). The velocity-loop robust controller is specified by Eq. (10). The position-loop P controller gain is assigned a value of 5452.273, while the three parameters of the feedforward compensation are 1.642x10^{-4}, 1.296x10^{-5}, and 1.653x10^{-9}, respectively. $T_{th} = 10.15$ and $R = 0.2$.

Based on Eq. (3) and Eq. (4), the simulated thrust ripple parameters are designed as $P = 0.015$, $q = 1,2,3,4,6$, $A_r = [0.03, 0.003, 0.1, 0.01, 0.015, 0.004, 0.03, 0.003, 0.03, 0.003]^T$ as the reference value. This thrust ripple has sufficient complexity to rigorously validate the performance of the proposed method.

4.1 Verification of Measurement-Output Reconfiguration for Enhanced Parameter Estimation

To illustrate that the measured output reconfiguration for RLS in the IARC framework can estimate the model parameters of thrust ripple more accurately, the conventional IARC method is selected as the comparative group. For fairness, the conventional IARC method differs from IARC-MORRLS by utilizing a low-pass filtered total control signal as the measured output and by eliminating the variable-gain mechanism, with all other simulation conditions kept the same. A second-order Butterworth low-pass filter was used to achieve low-pass filtering with a bandwidth of 3000 Hz.

First, two complete S-curve trajectory cycles of the motion were executed with the thrust ripple compensation deactivated. Thrust ripple excitation was initiated at $t = 2.0\ s$. Fig. 8 demonstrates the 12P12S PMLM's control performance before and after thrust ripple introduction. The maximum tracking error under the composite control strategy presented in Fig. 6 is 0.18 μm, whereas after thrust ripple introduction, it deteriorates to 297.70 μm.

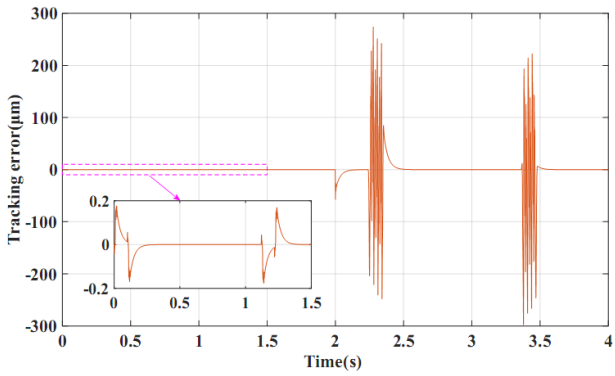

Figure 8. Control performance of composite control method and the effect of thrust ripple on tracking error

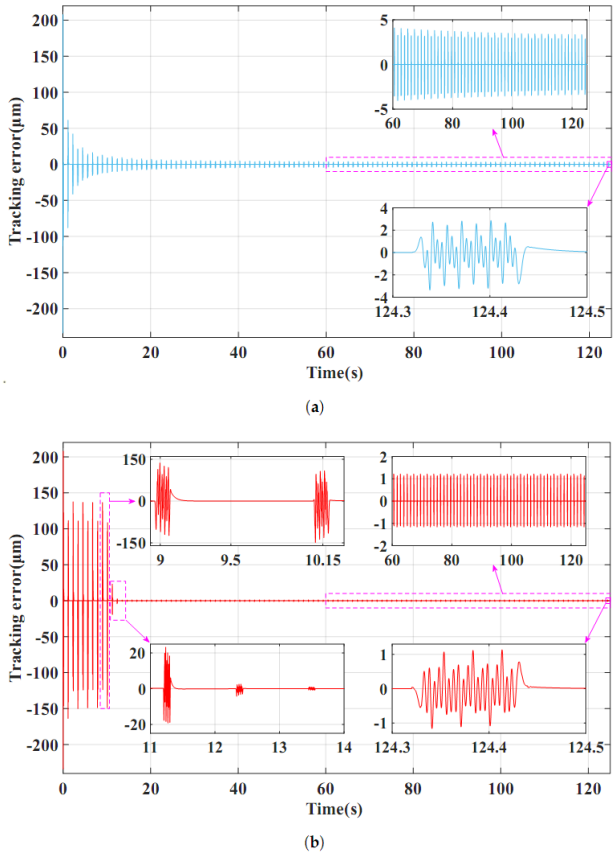

Figure 9. Thrust ripple compensation effectiveness. (**a**) Conventional IARC. (**b**) IARC-MORRLS

Then, enable the thrust ripple compensation. All parameters to be estimated are initialized to 10^{-6}; $p_0 = 10^6$. The parameter bounds in Eq. (15) are set to $\Theta_{\min} = 0.15$ and $\Theta_{\max} = 0.15$, and the parameter update rate limit Θ_m is set to 0.001. The suppression effect of the proposed IARC-MORRLS method and pure IARC method on the given thrust ripple after 125 seconds of repeated reference trajectory execution are shown in Fig. 9. The parameter estimation results are illustrated in Fig. 10.

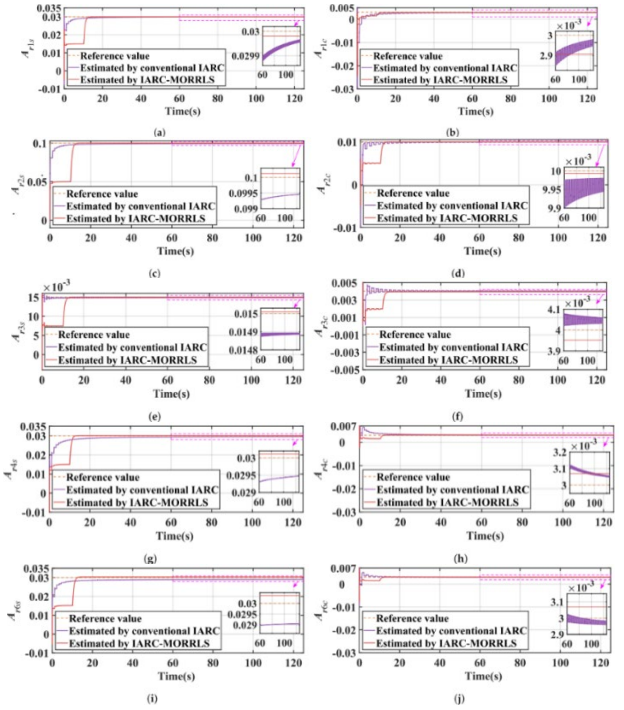

Figure 10. Thrust ripple parameter estimation results. (**a**) A_{r1s}. (**b**) A_{r1c}. (**c**) A_{r2s}. (**d**) A_{r2c}. (**e**) A_{r3s}. (**f**) A_{r3c}. (**g**) A_{r4s}. (**h**) A_{r4c}. (**i**) A_{r6s}. (**j**) A_{r6c}.

For the IARC-MORRLS method, the thrust ripple parameter estimation achieves preliminary convergence after 4.65 s, reaching about half of their reference values. After T_{th} s, the parameter estimation continues and ultimately achieves steady-state convergence at 24.15 s. For the conventional IARC method, the parameter estimation converges after 35.95 s. Compared to the conventional IARC method, the proposed method demonstrates superior estimation accuracy for parameters associated with dominant thrust ripple harmonics, notably A_{r2s} , A_{r4s} , A_{r6s} .

Fig. 11(a) shows the thrust ripple compensation signal after the preliminary parameter convergence. At $t = 3.3778$ s, the compensation signal amplitude is $7.755\text{x}10^{-1}$, while the thrust ripple amplitude measures $1.565\text{x}10^{-1}$, approximately twice the magnitude of the compensation signal. Fig. 11(b) and Fig. 11(c) demonstrates effective thrust ripple compensation achieved by the IARC-MORRLS method after the steady-state parameter convergence, with a maximum estimation error of only $6.804\text{x}10^{-4}$. In contrast, the maximum thrust ripple estimation error is $2.660\text{x}10^{-3}$ after applying the conventional IARC method.

Tracking errors were recorded over a 2.0 s duration under uncompensated thrust ripple conditions. After activating the compensation scheme and achieving parameter convergence, experimental data were acquired for an additional 2.0 s interval. Tracking performance was evaluated using the maximum absolute error (MAE) and root-mean-square error (RMSE) metrics. Table 1 shows the quantitative comparison results. The implementation of the IARC-MORRLS method achieves reductions of 99.6% in motion tracking MAE and

99.5% in RMSE, while demonstrating enhanced thrust ripple suppression compared to the conventional IARC method.

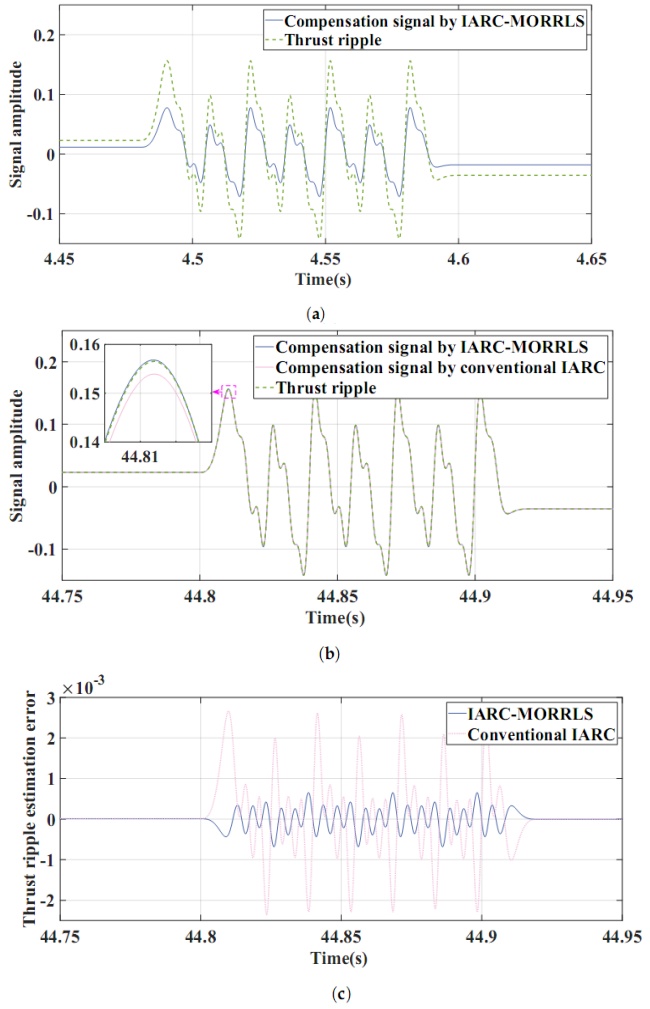

Figure 11. Thrust ripple compensation signal. (**a**) After the first-stage convergence of IARC-MORRLS. (**b**) After complete convergence of IARC-MORRLS and conventional IARC. (**c**) Thrust ripple estimation error of IARC-MORRLS and conventional IARC.

As shown in Figs. 10 and 11, without the proposed variable-gain mechanism, the IARC-MORRLS method can only attenuate 50% of the thrust ripple after parameter estimation completes preliminary convergence. With the variable-gain mechanism enabled, the proposed method achieves more accurate parameter estimation and better thrust ripple suppression after steady-state convergence compared with the conventional IARC method. This result clearlydemonstrates the effectiveness of the measurement-output reconfigured RLS algorithm.

Table 1. Quantitative analysis of simulation results

Metrics	Without TRC[1]	With TRC	
		Conventional IARC	IARC-MORRLS
MAE(μm)	297.70	3.35	1.21
RMSE(μm)	33.13	0.48	0.17

[1]TRC: Thrust Ripple Compensation

4.2 Verification of the Improved Projection Mapping

When applying the proposed method with deactivated slope-judgment mechanism specified in Eq. (17), the estimated thrust ripple parameters exhibit significant oscillations at the bounds defined in Eq. (15) during initial adaptation due to unconstrained update rates, as shown in Fig. 12(a). In contrast, activating the slope-judgment mechanism eliminates oscillations and facilitates smoother convergence, as demonstrated in Fig. 12(b).

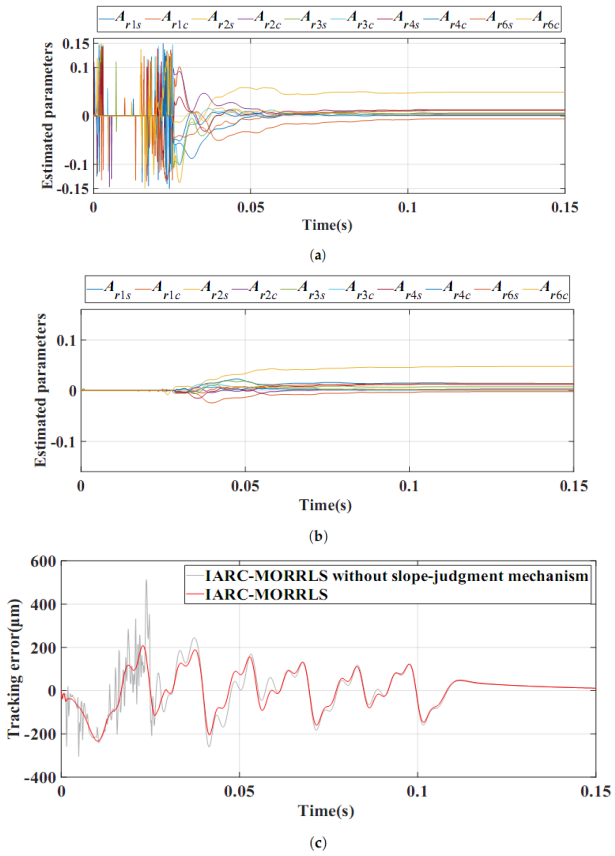

Figure 12. Estimation results of thrust ripple parameters with corresponding tracking errors when using the IARC-MORRLS method. (**a**) When the slope-judgment mechanism is deactivated. (**b**) When the slope-judgment mechanism is activated. (**c**) The tracking errors corresponding to the two parameter adaptation cases.

Fig. 12(c) shows tracking errors for both parameter adaptation cases. Disabling the slope-judgment mechanism generates pronounced oscillations during motor operation, yielding a 513.43 μm maximum tracking error that is 72.5% higher than the thrust-ripple-induced error in Fig. 8.

Activating the slope-judgment mechanism reduces maximum tracking error to 234.01 μm, the improved projection mapping thus effectively suppresses ripple and stabilizes the system.

5. Experimental Verification

To further verify the superiority of the proposed method in thrust ripple suppression, the experimental platform shown in Fig. 13 was constructed. As mentioned in Section 2, the experimental plant incorporates a 12P12S PMLM driven by a Copley driver, with position feedback resolution of 50 nm provided by a Renishaw's grating scale. The real-time control platform employs a dSPACE MicroLabBox operating at a 10 kHz sampling frequency, which executes the proposed control method. The human-machine interface, developed using the dSPACE ControlDesk software installed on the host computer, facilitates real-time monitoring of motor operational states and dynamic control parameter adjustment. Motion reference adopts the third-order S-curve profile from Fig. 7, modified with a stroke of 30 mm, peak velocity of 0.1 m/s and peak acceleration of 10 m/s².

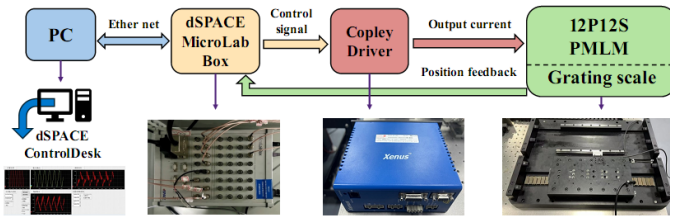

Figure 13. Experimental setup of the 12P12S PMLM motion stage

The velocity-loop controller still employs the robust controller shown in Eq. (10). Due to discrepancies between the practical model and the nominal model used during simulation, and the other parameters are set differently: the position-loop controller gain is set to 1440.452; the third-order feedforward parameters are 9.72×10^{-5}, 8.50×10^{-6}, and 5.65×10^{-9} respectively.

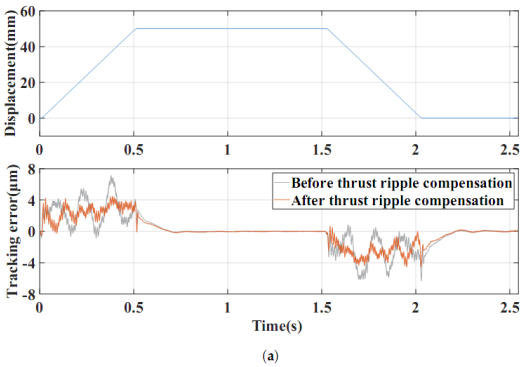

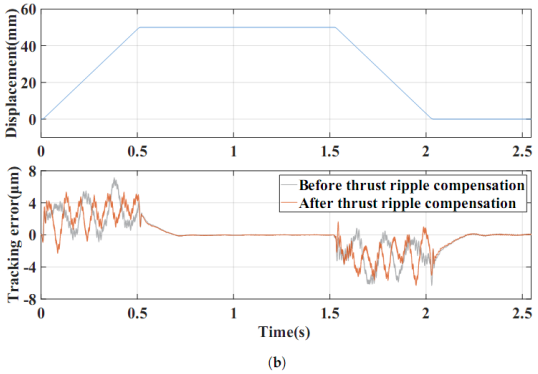

Figure 14. Experimental results of thrust ripple compensation effectiveness after complete convergence of the parameter estimation. (a) IARC-MORRLS. (b) Conventional IARC.

Experiments independently evaluated the proposed IARC-MORRLS and conventional IARC methods. For the conventional method, the low-pass filter bandwidth was set to 800 Hz. Fig. 14 and Table 2 summarize the motion control performance of both methods post-convergence. During constant-velocity operation, the proposed method reduces thrust-ripple-induced tracking error by 36.2% in MAE and 15.8% in RMSE, while also significantly reducing the peak-to-peak value of the tracking error curve. Furthermore, it exhibits enhanced performance compared to the conventional IARC method, demonstrating error mitigation trends consistent with simulation results.

Table 2. Quantitative analysis of experimental results

Metrics	Without TRC[1]	With TRC	
		Conventional IARC	IARC-MORRLS
MAE(μm)	7.15	6.30	4.56
RMSE(μm)	2.02	1.96	1.70

[1]TRC: Thrust Ripple Compensation

Experimental motion control results reveal significant deviations between experimental and simulation outcomes, primarily caused by discrepancies in nominal versus actual plant dynamics as well as nonlinear amplitude-phase characteristics of the thrust ripple in the 12P12S PMLM. Nevertheless, combining the previous simulation analysis and experimental verification illustrate the effectiveness and advantages of the proposed IARC-MORRLS method.

The experimental results strongly validate the effectiveness of the control method proposed in this paper. However, to provide a more comprehensive understanding of the system characteristics and algorithm design, certain aspects require further discussion.

1. The rationale for selecting specific harmonic orders to model the thrust ripple is fundamentally based on empirical data analysis and strict validation requirements. By applying a Fast Fourier Transform analysis to the raw experimental measurement data, it is clearly observed that the amplitudes

of the 1st, 2nd, 3rd, 4th, and 6th harmonic components are predominantly large compared to other high-order frequencies. Extracting these specific major orders allows for the establishment of an accurate and highly representative mathematical model of the physical thrust ripple. Furthermore, deliberately adopting a complex harmonic model provides a rigorous testing environment to evaluate the performance limits of the algorithm. This effectively demonstrates the robust capability of the proposed method to execute simultaneous and accurate multi-parameter identification under complicated disturbance conditions.

2. The general applicability of the proposed method across different velocities is another crucial aspect. The rationale for utilizing the low-speed condition as the primary experimental benchmark is that it represents the most severe worst-case scenario for precision motion control. At low speeds, the system is subjected to low-frequency thrust ripples strongly coupled with severe nonlinear friction such as the Stribeck effect. As velocity increases, the frequency of thrust ripples increases proportionally and is inherently smoothed out by the natural inertia of the mechanical mover, which acts as a natural low-pass filter. Simultaneously, the complex nonlinear friction transitions into simpler linear viscous friction. Because medium-to-high-speed operations represent a dynamically more benign environment, an algorithm proven effective in the stringent low-speed scenario will inherently maintain its validity and robustness at higher velocities.

3. The computational overhead of the proposed method is relatively low compared to the conventional approach. The dominant computational burden in both methods stems from the parameter estimator and the slope judgment mechanism. Since these core components are shared, their baseline computational costs are identical. The fundamental structural difference is that the conventional method requires the additional calculation of a discrete second-order Butterworth low-pass filter, demanding approximately five multiplications and four additions per sampling period. In contrast, the proposed method eliminates the need for this low-pass filter and instead computes a variable gain mechanism. The exponential function in this mechanism can be executed recursively in discrete time steps, requiring only one multiplication and one subtraction per step. Therefore, the computational overhead of the variable gain mechanism is strictly lower than that of the Butterworth filter, allowing the proposed method to significantly improve steady-state convergence performance without introducing any extra computational burden.

6. Conclusions

The primary contribution of this paper is the proposal of an IARC method with a measured-output-reconfigured recursive least squares to address motion control performance deterioration in PMLMs due to thrust ripple. The dual-loop feedback control structure with an H∞ robust controller is designed. Combined with parameterized feedforward compensation, this composite scheme achieves the robustness of the conventional IARC method while enabling fast reference trajectory tracking. Conventional IARC's RLS measured output is redefined as the feedback control signal, eliminating the essential low-pass filter and its adverse effects on parameter adaptation. The variable-gain mechanism ensures parameter estimation converges to better accuracy, enhancing thrust ripple compensation efficacy, while the projection mapping with slope-judgment mechanism mitigates initial estimation-phase oscillation effects on control system stability. Simulations on a nominal model of 12P12S PMLM motion stage demonstrate 99.6% and 99.5% reductions in MAE and RMSE, respectively, compared to uncompensated systems. Experimental validation shows 36.2% lower MAE and 15.8% lower RMSE after compensation. Both simulation and experimental results prove the superiority of the proposed method over the conventional IARC method, confirming its effectiveness in enhancing precision motion control. In future work, we will investigate thrust ripple nonlinear dynamics to enhance the precision of motion control for linear motor systems.

Acknowledgments

This research was funded by School-Enterprise Cooperation Project for Domestic Visiting Engineer in Higher Education Institutions (Grant No. FG2023148), National Natural Science Foundation of China (Grant No U23A20645), the Ningbo Science and Technology Innovation 2025 Major Special Project (Grant No. 2022Z193 and 2023Z007), Ningbo Key R&D Program and "Revealing the Leader on the List" (Grant No. 2023Z025), Ningbo Key R&D Program of "Science and Innovation Yongjiang 2035" (Grant No. 2025Z011).

References

[1] S. Riaz, C. W. Yin, R. Qi, B. Q. Li, S. Ali, and K. Shehzad, "Design of Predefined Time Convergent Sliding Mode Control for a Nonlinear PMLM Position System, " Electronics 12, 813 (2023).

[2] X. J. Yang, B. F. Song, and J. L. Xuan, "Effects of the mechanical vibrations on the thrust force characteristics for the PMLM driven motion system, " Mech. Syst. Signal Pr. 175, 109110 (2022).

[3] R. D. Zhi, B. Liu, G. Lv, L. L. Cui, and T. Zhou, "Characteristics Analysis of Novel Transverse Flux Linear Synchronous Motor for Maglev Transportation, " IEEE Trans. Transp. Electrific. 9, 4104-4112 (2023).

[4] Y. B. Liu, W. C. Sun, and H. J. Gao, "High Precision Robust Control for Periodic Tasks of Linear Motor via B-Spline Wavelet Neural Network Observer, " IEEE Trans. Ind. Electron. 69, 8255-8263 (2022).

[5] J. Wang, X. Chen, Q. Y. Chen, Q. Xi, and H. Y. Sun, "Position Detection System for Moving-Magnet Linear Motors Based on a Magnetoresistive Sensor Array, " Sensors 25, 1019 (2025).

[6] L. Z. Zeng, X. D. Chen, X. Q. Li, W. Jiang, and X. Luo, "A Thrust Force Analysis Method for Permanent Magnet

Linear Motor Using Schwarz-Christoffel Mapping and Considering Slotting Effect, End Effect, and Magnet Shape, ” IEEE Trans. Magn. 51, 1-9 (2015).
[7] X. Z. Wang, F. X. Chen, R. F. Zhu, X. L. Huang, N. Sang, G. L. Yang, and C. Zhang, “A Review on Disturbance Analysis and Suppression for Permanent Magnet Linear Synchronous Motor, ” Actuators 10, 77 (2021).
[8] J. H. Kwon, J. K. Kim, and E. S. Jeon, “Shape Optimization of Discontinuous Armature Arrangement PMLSM for Reduction of Thrust Ripple, ” Appl. Sci. 11, 11066 (2021).
[9] X. Z. Xu, L. M. Jia, S. Y. Jiang, and H. C. Feng, “Mover structure optimization and performance improvement for halbach consequent-pole PM synchronous linear motors with flux barrier, ” J. Magn. Magn. Mater. 591, 171692 (2024).
[10] Z. Chen, W. B. Kong, Y. Zhou, R. H. Qu, and V. Fedida, “Thrust force ripple reduction of H-LVPMM based on dynamic harmonic current compensation, ” IET Electr. Power Appl. 14, 226-233 (2020).
[11] Y. W. Zhu and Y. H. Cho, “Thrust Ripples Suppression of Permanent Magnet Linear Synchronous Motor, ” IEEE Trans. Magn. 43, 2537-2539 (2007).
[12] K. Zuo, Y. Hong, J. Yang, L. Xu, H. T. Qi, B. L. Li, H. Liu, and L. Y. Liu, “Thrust Coordinated Assignment and Ripple Suppression of a Multiple Modular Permanent Magnet Linear Synchronous Motor Based on Model Predictive Thrust Control, ” Energies 16, 5368 (2023).
[13] J. C. Yuan, J. S. Li, and Y. Ding, “Modified modeling and internal model control method of thrust ripples in PMLSMs for ultraprecision air-bearing linear feed systems, ” Precis. Eng. 85, 102–112 (2024).
[14] X. W. Fu, X. F. Yang, and Z. Y. Chen, “A New Linear Motor Force Ripple Compensation Method Based on Inverse Model Iterative Learning and Robust Disturbance Observer,” Complexity 2018, 9647257 (2018).
[15] W. Zhang, N. Nan, Y. Yang, W. Zhong, and Y. Chen, “Force ripple compensation in a PMLSM position servo system using periodic adaptive learning control,” ISA Trans. 95, 266–277 (2019).
[16] S. Lee, Y. S. Kwon, J. H. Jung, K. Kang, C. H. Kim, and J. Y. Yoon, “Identification-Based Simultaneous Reduction of Tangential and Normal Force Ripples in PMLSMs Under Dynamic Operation,” IEEE Transactions on Industrial Electronics, vol. 73, no. 5, pp. 7460-7471, 2026.
[17] G. Zhang, X. Zhao, Q. Wang, D. Ding, B. Li, G. Wang, and D. Xu, “PR Internal Mode Extended State Observer-Based Iterative Learning Control for Thrust Ripple Suppression of PMLSM Drives, ” IEEE Transactions on Power Electronics, vol. 39, no. 8, pp. 10095-10105, 2024.
[18] L. Lu, Z. Chen, B. Yao, and Q. F. Wang, “Desired Compensation Adaptive Robust Control of a Linear-Motor-Driven Precision Industrial Gantry with Improved Cogging Force Compensation, ” IEEE/ASME Trans. Mechatron. 13, 617–624 (2008).
[19] 19 M. X. Yuan, Z. Chen, B. Yao, and X. Y. Liu, “Fast and Accurate Motion Tracking of a Linear Motor System Under Kinematic and Dynamic Constraints: An Integrated Planning and Control Approach, ” IEEE Trans. Contr. Syst. Technol. 29, 804–811 (2021).
[20] R. C. Tao, J. Ma, and H. Zhao, “Torque Ripple Minimization in PMSM Based on an Indirect Adaptive Robust Controller, ” Math. Probl. Eng. 2017, 9512351 (2017).
[21] A. Mohanty and B. Yao, “Indirect Adaptive Robust Control of Hydraulic Manipulators with Accurate Parameter Estimates, ” IEEE Trans. Contr. Syst. Technol. 19, 567–575 (2011).
[22] Z. Chen, B. Yao, and Q. F. Wang, “μ-Synthesis-Based Adaptive Robust Control of Linear Motor Driven Stages with High-Frequency Dynamics: A Case Study, ” IEEE/ASME Trans. Mechatron. 20, 1482–1490 (2015).
[23] J. T. Yang, J. H. Chen, Z. Y. Cai, W. Y. Yan, W. Liu, J. Zhang, J. J. Qiao, G. L. Yang, and C. Zhang, “Design and Optimization of a Novel Permanent Magnet Linear Motor with the Same Number of Poles and Slots, ” IEEE Trans. Ind. Appl. 61, 16–24 (2025).
[24] W. Z. Wang, C. Zhang, N. Sang, B. Zhao, Z. Tian, S. L. Chen, and G. L. Yang, “Segmented ternary composite control method considering time delay for high-speed and high-precision linear motor, ” Precis. Eng. 88, 584–594 (2024).
[25] L. Bascetta, P. Rocco, and G. Magnani, “Force Ripple Compensation in Linear Motors Based on Closed-Loop Position-Dependent Identification, ” IEEE/ASME Trans. Mechatron. 15, 349–359 (2010).
[26] B. Yao, C. X. Hu, L. Lu, and Q. F. Wang, “Adaptive Robust Precision Motion Control of a High-Speed Industrial Gantry with Cogging Force Compensations, ” IEEE Trans. Contr. Syst. Technol. 19, 1149–1159 (2011).
[27] L. Biagiotti and C. Melchiorri, Trajectory Planning for Automatic Machines and Robots (Springer, Berlin Heidelberg, 2008).
[28] L. Y. Dai, X. Li, Y. Zhu, and M. Zhang, “Auto-tuning of model-based feedforward controller by feedback control signal in ultraprecision motion systems, ” Mech. Syst. Signal Pr. 142, 106764 (2020).
[29] Z. Chen, B. Yao, and Q. Wang, “Adaptive Robust Precision Motion Control of Linear Motors with Integrated Compensation of Nonlinearities and Bearing Flexible Modes, ” IEEE Trans. Ind. Inf. 9, 965–973 (2013).